Size-Dependent Detachment-Limited Decay Kinetics of Two-Dimensional TiN Islands on TiN(111)

S. Kodambaka, V. Petrova, S.V. Khare, D. Gall, A. Rockett, I. Petrov, and J. E. Greene
Department of Materials Science and the Frederick Seitz Materials Research Laboratory, University of Illinois, 104 South Goodwin Avenue, Urbana, Illinois 61801
(Received 23 June 2002; published 2 October 2002)

In situ high-temperature ($T_a = 1050$–1250 K) scanning tunneling microscopy was used to determine the coarsening and decay kinetics of two-dimensional TiN adatom and vacancy islands on atomically smooth TiN(111) terraces. We report the first observation of an abrupt decrease in decay rates, irrespective of T_a, of adatom islands with areas less than a critical value of 1600 Å^2. However, no decay rate transition was observed for vacancy islands. We attribute the size-dependent island decay behavior, which is consistent with detachment-limited kinetics, to anisotropic attachment and detachment barriers.

DOI: 10.1103/PhysRevLett.89.176102 PACS numbers: 68.35.Md, 68.35.Fx, 68.37.Ef, 82.45.Mp

B1-NaCl structure TiN is widely used as a hard wear-resistant coating on cutting tools, a diffusion-barrier in microelectronic devices, a corrosion-resistant coating on mechanical components, and an abrasion-resistant layer on optical components. Even though the elastic and diffusion-barrier properties of TiN are known to be highly anisotropic, and hence depend strongly upon film texture, little is known regarding the mechanisms and reaction paths leading to the development of preferred orientation in polycrystalline TiN layers. Efforts to model these processes [1] require, as input, adatom transport parameters (adatom surface diffusion and island edge attachment and detachment energies), the step-edge Ehrlich barrier, the adatom formation energy and the step formation energy, all as a function of orientation. Unfortunately, relatively little data, either experimental or theoretical, are available concerning these parameters [2,3]. Here, we focus on adatom transport on TiN(111) surfaces.

Modeling of experimentally determined two-dimensional island coarsening and decay (Ostwald ripening) rates on well-defined atomically flat surfaces as a function of annealing time t_a and temperature T_a provides a means to probe early-stage film growth mechanisms and to determine adatom surface transport parameters [4]. Ostwald ripening [5] is a phenomenon in which larger islands on a surface grow at the expense of smaller neighboring islands. The process is described by the Gibbs-Thomson equation [5] in which the equilibrium free adatom concentration ρ^{eq} associated with an island is related to the equilibrium island curvature κ through the expression

$$\rho^{\mathrm{eq}} = \rho_{\infty}^{\mathrm{eq}} \exp\left(\frac{\tilde{\beta}\kappa\Omega}{kT_a}\right), \tag{1}$$

where $\rho_{\infty}^{\mathrm{eq}}$ is the equilibrium free adatom concentration associated with a straight step, $\tilde{\beta}$ is the step stiffness, and Ω is the unit molecular area. Smaller islands have higher curvatures, and hence higher adatom concentrations than larger islands resulting in mass transfer from smaller to larger islands.

Experimental coarsening studies have mostly been carried out on isotropic, or near-isotropic, surfaces such as Ag(111) [6], Cu(111) [7], Cu(001) [8], and TiN(001) [2] and modeled based upon isotropic adatom transport. Si(001), although anisotropic in nature, exhibits isotropic coarsening/decay kinetics [9]. Deviation from isotropic coarsening/decay kinetics has, so far, been observed only on Ag(110) [10] and Au(110) [11]. On isotropic metal surfaces, novel adatom transport phenomena have been observed and reasonably well understood [12]. However, adatom transport phenomena on anisotropic surfaces are still not well investigated.

In this Letter, we present results from an *in situ* high-temperature ($T_a = 1050$–1250 K) scanning tunneling microscopy (STM) study of the coarsening kinetics of two-dimensional (2D) TiN adatom islands on highly anisotropic TiN(111) surfaces. We observe a novel behavior: an abrupt decrease in island decay rates, irrespective of T_a, for islands with areas A less than a critical value $A_c \simeq 1600$ Å^2. In contrast, the decay of 2D TiN(111) vacancy islands does not exhibit this transition. The coarsening/decay kinetics of both adatom and vacancy islands are consistent with a detachment-limited mechanism. From temperature-dependent decay rates, we obtain activation energies E_a for TiN(111) adatom island decay of 3.3 ± 0.4 eV ($A < A_c$) and 2.3 ± 0.6 eV ($A > A_c$). We suggest that the transition in adatom island decay kinetics is due to anisotropic attachment/detachment barriers.

Epitaxial TiN(111) layers, 2000 Å thick, were grown on $Al_2O_3(11\bar{2}0)$ by ultrahigh vacuum (UHV) magnetically unbalanced magnetron sputter deposition [13] using the procedure described in Ref. [14]. The samples were transferred to a UHV multichamber system, with a base pressure of 2×10^{-10} Torr, containing a variable-temperature

Omicron scanning tunneling microscope. The system is equipped with facilities for electron-beam evaporation, ion etching, Auger electron spectroscopy (AES), and low energy electron diffraction (LEED). Sample temperatures were measured by optical pyrometry and calibrated using temperature-dependent TiN emissivity data obtained by spectroscopic ellipsometry. The TiN(111) layers were degassed in UHV at 1073 K, where the N_2 vapor pressure over TiN is less than 10^{-10} Torr [3], for approximately 1200 s. Epitaxial TiN(111) buffer layers, 50–100 Å thick, were then deposited at 1023 K in the STM chamber by reactive evaporation from Ti rods (99.999% purity) in N_2 (99.999% purity) at 1×10^{-7} Torr. The buffer layers were annealed in N_2 for 4 h at a temperature $T_a \simeq 1100$ K. This procedure results in sharp 1×1 LEED patterns corresponding to an in-plane atomic spacing of 2.99 Å and an STM-measured step height of 2.4 Å, both equal to expected values for bulk TiN [3]. AES analyses show that the samples contain $\simeq 2$ mole % oxygen, probably in the form of TiO which is isostructural [3] and mutually soluble with TiN.

Partial TiN(111) bilayers (BL) [15] with coverages of 0.1–0.8 BL were deposited on TiN(111)/$Al_2O_3(11\bar{2}0)$ substrates by reactive evaporation at room temperature. The samples were then annealed *in situ* at $T_a =$ 1050–1250 K in 1×10^{-7} Torr N_2 for times $t_a = 1$–2 h. This results in surfaces with $\simeq 500$-Å-wide atomically smooth terraces (separated by bilayer-height steps) with truncated hexagonal-shaped 2D TiN(111) adatom islands for coverages <0.4 BL and vacancy islands at higher coverages. Both adatom and vacancy islands have average areas ranging from 9×10^3 to 2×10^5 Å^2. At each T_a, STM images (typically 300 per sequence) were acquired as a function of t_a at a constant rate (18 to 44 s/frame). Typical tunneling conditions were 0.4–0.6 nA at -3.5 V. The sample and tip were allowed to thermally stabilize at T_a for 2 to 3 h prior to obtaining the STM images. Pixel resolution in the images varied from 2×2 to 5×5 Å^2. For each of the measurement sequences, island boundaries were identified and island areas determined from the STM images using Image SXM [16], an image processing software. Scan sizes, scan rates, and tunneling parameters were varied to check for tip induced effects. No such effects were observed in the results presented here.

Figures 1(a) and 1(b) show representative STM images (1660×1660 Å^2) of 2D TiN(111) adatom and vacancy islands acquired at 34 s/frame during annealing at $T_a =$ 1211 K for times $t_a = 0$ and 82 min, respectively. The truncated hexagonal shapes of the TiN(111) islands indicate that they are highly anisotropic. Most of the islands observed at $t_a = 0$ (e.g., adatom islands 1–6 and vacancy island 8) have disappeared by $t_a = 82$ min, leaving only the largest island, labeled 7. Typical results showing the areas A of adatom islands 1, 4, and 6 vs t_a are plotted in Fig. 2(a). The areas of all adatom islands were found to decrease linearly with t_a at a constant decay rate dA/dt_a,

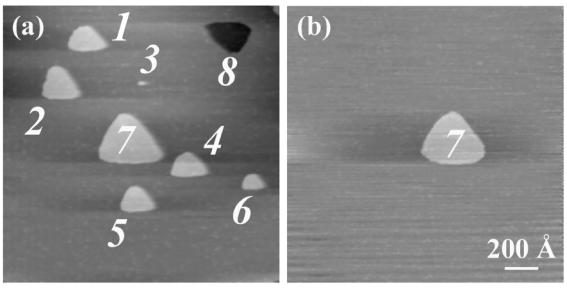

FIG. 1. Representative STM images (1660×1660 Å^2) of 2D TiN adatom (1)–(7) and vacancy (8) islands on an atomically smooth TiN(111) terrace. The images were acquired at 34 s/frame at times $t_a =$ (a) 0 and (b) 82 min during annealing at $T_a = 1211$ K.

independent of local environment, with an abrupt decrease in slope at $A = A_c$. This is illustrated more clearly for island 6 in the inset of Fig. 2(a). dA/dt_a values for all adatom islands with $A > A_c$ were found to be a factor of 3 to 20, depending monotonically on T_a, higher than the same islands with $A < A_c$.

Figure 2(b) is a plot of A vs t_a for vacancy island 8 in Fig. 1(a). dA/dt_a remains constant, with no slope transition, over the entire decay process. A vs t_a data in Figs. 2(a) and 2(b) are typical of STM results obtained from over 80 large ($A > A_c$) and 40 small ($A < A_c$) adatom islands and 5 vacancy islands observed at temperatures in the range 1050–1250 K.

In classical mean-field theory, the decay rate dA/dt_a of an isotropic (circular) island exhibiting detachment-limited kinetics is given by $dA/dt_a = -K_d L \Omega[\rho^{\mathrm{eq}} - \rho_s^{\mathrm{eq}}]$ [17], where K_d is a temperature-dependent adatom attachment/detachment rate coefficient, L is the island perimeter, and ρ_s^{eq} is the equilibrium free adatom concentration on the surface. For an anisotropic island, where K_d may depend on step orientation φ, dA/dt_a is given by

$$\frac{dA}{dt_a} = -\Omega \int_0^{2\pi} d\varphi\, r(\varphi) K_d(\varphi)[\rho^{\mathrm{eq}} - \rho_s^{\mathrm{eq}}]. \qquad (2)$$

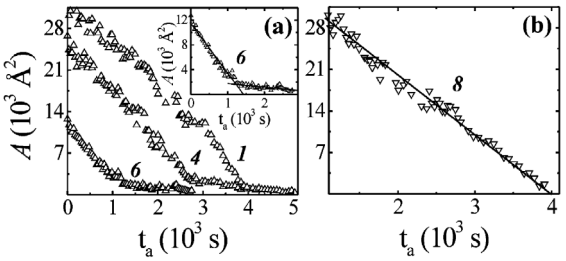

FIG. 2. (a) Island area A vs annealing time t_a for 2D adatom islands 1, 4, and 6 at $T_a = 1211$ K in Fig. 1(a). A discontinuous decrease in decay rates was observed at a critical area A_c. Inset: A vs t_a plot for island 6. (b) A vs t_a for vacancy island 8 in Fig. 1(a) . The solid lines in each case are linear least-squares fits to the data.

$r(\varphi)$ in Eq. (2) is the radial distance from the island center to the edge as a function of azimuthal angle φ. In the pure detachment-limited regime, $\rho_s^{\rm eq} = \rho_\infty^{\rm eq}$ and, assuming that the exponential term in Eq. (1), $\exp(\tilde{\beta}\kappa\Omega/kT_a)$, can be expanded to the first two terms [18], we obtain

$$\frac{dA}{dt_a} = -\Omega\rho_\infty^{\rm eq}\int_0^{2\pi} d\varphi r(\varphi)K_d(\varphi)\left(\frac{\tilde{\beta}\kappa\Omega}{kT_a}\right). \qquad (3)$$

Since the equilibrium island chemical potential $\mu = \tilde{\beta}\kappa\Omega$ is independent of step orientation and depends only on island size, μ can be represented in terms of a size- and orientation-independent parameter B as $\mu = B\Omega/r_{\rm avg}$ [19], where $r_{\rm avg} = (A/\pi)^{1/2}$ is the orientation-averaged island radius. B determines the energy scale of the island equilibrium chemical potential and is a constant for the equilibrium shape. Rewriting Eq. (3) in terms of B yields

$$\frac{dA}{dt_a} = -\left(\frac{B\Omega^2\rho_\infty^{\rm eq}}{r_{\rm avg}kT_a}\right)\int_0^{2\pi} d\varphi[r(\varphi)K_d(\varphi)]. \qquad (4)$$

We note that Eq. (4), which shows that dA/dt_a is independent of island size for a given T_a in the detachment-limited regime, is valid even for anisotropic equilibrium-shaped islands. In the case of TiN(111), we find experimentally that while dA/dt_a is constant, indicative of detachment-limited kinetics, its value is larger at $A > A_c$ than at $A < A_c$ suggesting an abrupt change in the parameters B or $K_d(\varphi)$ at A_c.

As an initial step toward understanding these results, we analyzed island shapes as a function of area $A(t_a)$ during the decay process. The equilibrium shape of all 2D TiN(111) islands (whether composed of adatoms or vacancies) consists of two alternating ⟨110⟩ step edges labeled S_1 and S_2 as illustrated in Fig. 3(a). R_1 and R_2 are the radial distances to the respective step edges measured with respect to the center of the equilibrium island shape.

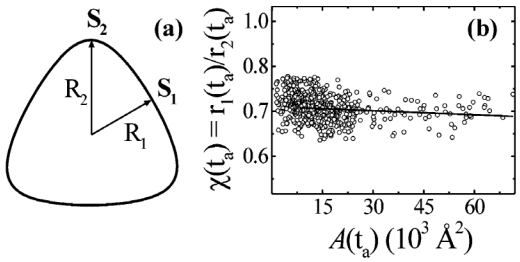

FIG. 3. (a) Equilibrium shape of a 2D TiN(111) island. The two ⟨110⟩ steps are labeled as S_1 and S_2 and the corresponding radial distances from the center of the island are R_1 and R_2, respectively. (b) $\chi(t_a) = [r_1(t_a)/r_2(t_a)]$ vs $A(t_a)$ plot for islands during decay at $T_a = 1178$–1248 K, where $r_1(t_a)$ and $r_2(t_a)$ are the time-dependent radial distances from the center of the island to S_1 and S_2 steps, respectively. The solid line is the least-squares fit to the data.

From the STM measurements of island shapes observed during the decay of each island, the ratios $\chi(t_a) \equiv r_1(t_a)/r_2(t_a)$, where $r_1(t_a)$ and $r_2(t_a)$ are time-dependent radial distances measured from the center of the island to S_1 and S_2 steps respectively, were determined.

Figure 3(b) is a plot of $\chi(t_a)$ vs $A(t_a)$ for 32 adatom islands, with $A(t_a = 0) > 8000$ Å^2. The data were obtained during annealing at $T_a = 1178$–1248 K. From a least-squares analysis of the data (solid line in Fig. 3(b)), we find that $\chi(t_a)$ remains constant at 0.73 ± 0.04. This result is nearly identical to the corresponding ratio of 0.72 ± 0.02 determined for equilibrium-shaped islands [3] indicating that the islands retain their equilibrium shape during coarsening/decay. This result, assuming that islands with $A < A_c$ also maintain their equilibrium shapes, implies that B is constant. Thus, from Eq. (4), the abrupt change in dA/dt_a must be due to an implicit island size-dependence in $K_d(\varphi)$ [20].

We determined dA/dt_a, using least-squares analysis, from the measured data for all adatom islands, at both $A \gg A_c$ and $A \ll A_c$. The point of intersection in the linear fits was found to be $A_c = 1600 \pm 470$ Å^2 corresponding to 220 ± 65 TiN molecules ($\Omega = 7.2$ Å^2), independent of T_a and the initial area of islands with $A > A_c$. Figure 4 is a plot of dA/dt_a for large ($A > A_c$) and small ($A < A_c$) adatom islands as a function of T_a. dA/dt_a, given by Eq. (4), is a function of the product of the thermally activated parameters $\rho_\infty^{\rm eq}$ and K_d. Thus, dA/dt_a can be expressed in the form $dA/dt_a \sim \exp(E_a/kT_a)$ with an activation barrier E_a. From the data, we obtain an activation energy $E_{\rm ad,small} = 3.3 \pm 0.4$ eV with a prefactor $\nu = 10^{13.3\pm1.6}$ s^{-1} for decay of small adatom islands and $E_{\rm ad,large} = 2.3 \pm 0.6$ eV with $\nu = 10^{9.6\pm2.5}$ s^{-1} for large adatom islands. dA/dt_a for five vacancy islands, also shown in Fig. 4 as open triangles, are comparable to, if not higher than, that of adatom

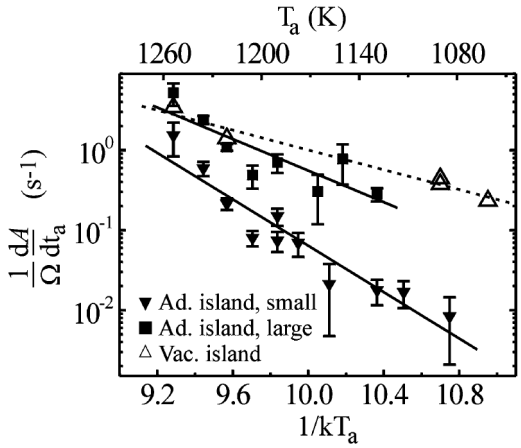

FIG. 4. Island decay rates dA/dt_a vs annealing temperature T_a for small ($A < A_c$, ▼) and large ($A > A_c$, ■) 2D TiN(111) adatom and vacancy (△) islands.

islands with $A > A_c$ indicating that the activation energy E_{vac} for decay of vacancy islands is $\leq E_{\text{ad,large}}$.

In the detachment-limited regime, $E_a = E_f + E_s + E_d$, where E_f, E_s, and E_d are the adatom formation energy, surface diffusion barrier, and attachment/detachment barrier, respectively. Since E_f and E_s are independent of island size, $(E_{\text{ad,small}} - E_{\text{ad,large}})$ corresponds to a difference in E_d values for small and large adatom islands.

It is reasonable to assume, based upon direct observations [21], that at relatively low temperatures, which is the case here where T_a varies from 0.33 to 0.39 of the TiN melting point in K [22], attachment/detachment occurs only at kink sites. Thus K_d, and hence E_d, depend on the kink density (number of kinks per unit step length), which in turn depends on the kink formation energy ε. For TiN(111), $\varepsilon_1 \simeq 0.43$ eV and $\varepsilon_2 \simeq 0.13$ eV, where ε_1 and ε_2 correspond to kink formation energies along S_1 and S_2 steps, respectively [3]. Thus, for large islands, attachment/detachment of diffusing species occurs preferentially along S_2 steps. By mapping the measured equilibrium shape of an island with $A \simeq A_c$ onto the TiN(111) 2D surface mesh, we find that islands with $A \leq A_c$ ($= 1600$ Å^2) are bounded by S_2 steps of length ≤ 4 atoms and S_1 steps of length ≤ 12 atoms. Kink formation along 4-atom-long S_2 steps involves removal of an atom to produce a double kink, which is energetically unfavorable. Thus, for islands with $A \leq A_c$, attachment/detachment of diffusing species occurs predominately along S_1 steps which have higher kink formation energies and, hence, higher E_{ad} values and lower decay rates as we observe. Despite the anisotropy in detachment barriers, the equilibrium shape is maintained during island decay by fast edge diffusion. In the case of vacancy islands, E_{vac} and, hence, E_d are independent of island size suggesting different pathways for attachment/detachment of adatom and vacancy islands.

In conclusion, we have measured the decay kinetics of 2D TiN adatom and vacancy islands on highly anisotropic TiN(111) surfaces using *in situ* high-temperature STM. We find an abrupt decrease in decay rates for adatom islands with areas A less than a critical value $A_c \simeq 1600$ Å^2, irrespective of T_a. However, no decay rate transition was observed for vacancy islands. The coarsening/decay kinetics of both adatom and vacancy islands on TiN(111) are consistent with a detachment-limited mechanism. From time- and temperature-dependent island area measurements, we obtain activation energies for TiN(111) adatom island decay of 3.3 ± 0.4 eV ($A < A_c$) and 2.3 ± 0.6 eV ($A > A_c$). These results provide the first evidence of a strong island size-dependence, and therefore a large anisotropy in attachment/detachment activation barriers. We expect this to be a general phenomenon applicable to 2D adatom island coarsening on all anisotropic surfaces.

The authors gratefully acknowledge the financial support of the U.S. Department of Energy (DOE), Division of Materials Science, under Contract No. DEFG02-91ER4539 through the University of Illinois Frederick Seitz Materials Research Laboratory (FS-MRL). We thank G. Ehrlich, T. L. Einstein, and N. C. Bartelt for their valuable suggestions and comments. We also appreciate the use of the facilities in the Center for Microanalysis of Materials, partially supported by DOE, at the FS-MRL.

[1] F. H. Baumann *et al.*, MRS Bull. **26**, 182 (2001).
[2] S. Kodambaka *et al.*, Surf. Rev. Lett. **7**, 589 (2000); Thin Solid Films **392**, 164 (2001).
[3] S. Kodambaka *et al.*, Phys. Rev. Lett. **88**, 146101 (2002), and references therein.
[4] M. Giesen, Prog. Surf. Sci. **68**, 1 (2001).
[5] W. W. Mullins, Interface Sci. **9**, 9 (2001), and references therein.
[6] K. Morgenstern, G. Rosenfeld, and G. Comsa, Phys. Rev. Lett. **76**, 2113 (1996); Surf. Sci. **441**, 289 (1999).
[7] G. S. Icking-Konert, M. Geisen, and H. Ibach, Surf. Sci. **398**, 37 (1998).
[8] J. B. Hannon *et al.*, Phys. Rev. Lett. **79**, 2506 (1997).
[9] N. C. Bartelt, W. Theis, and R. M. Tromp, Phys. Rev. B **54**, 11741 (1996).
[10] K. Morgenstern, E. Lægsgaard, I. Stensgaard, and F. Besenbacher, Phys. Rev. Lett. **83**, 1613 (1999); S. Rusponi *et al.*, Surf. Sci. **440**, 451 (1999).
[11] M. J. Rost, R. van Gastel, and J. W. M. Frenken, Phys. Rev. Lett. **84**, 1966 (2000); M. J. Rost, S. B. van Albada, and J. W. M. Frenken, *ibid.* **86**, 5938 (2001).
[12] Maozhi Li *et al.*, Phys. Rev. Lett. **86**, 2345 (2001); M. Giesen, G. Schulze Icking-Konert, and H. Ibach, Phys. Rev. Lett. **80**, 552 (1998); **82**, 3101 (1999); K. Morgenstern *et al.*, Phys. Rev. B **63**, 045412 (2001).
[13] I. Petrov *et al.*, J. Vac. Sci. Technol. A **10**, 3283 (1992).
[14] J. E. Greene *et al.*, Appl. Phys. Lett. **67**, 2928 (1995).
[15] The [111] direction in B1-NaCl structure TiN is polar, consisting of alternating layers of Ti and N atoms.
[16] Image SXM, developed by Professor Steve Barrett, Liverpool, United Kingdom (http://reg.ssci.liv.ac.uk).
[17] J. G. McLean *et al.*, Phys. Rev. B **55**, 1811 (1997).
[18] For TiN(111), based on the stiffness and curvature values from Ref. [3], the maximum uncertainties introduced due to this assumption are $\simeq 0.1\%$ at $A > A_c$ and $\simeq 2.5\%$ at $A < A_c$.
[19] S. Kodambaka *et al.*, Surf. Sci. **513**, 468 (2002).
[20] An alternate explanation assuming a difference in chemical compositions of islands with $A < A_c$ and $A > A_c$, resulting in the observed transition in island decay rates is not discussed here.
[21] L. Kuipers *et al.*, Phys. Rev. B **52**, 11 387 (1995); C. Pearson *et al.*, Phys. Rev. Lett. **74**, 2710 (1995).
[22] *CRC Handbook of Chemistry and Physics* (CRC Press, Cleveland, 2001), 82nd ed., pp. 4–91.